International Journal of Microwave and Wireless Technologies

cambridge.org/mrf

Research Paper

Cite this article: Norouzzadeh E, Chamaani S, Moll J, Kexel C, Nguyen DH, Hübner F, Bazrafshan B, Vogl TJ, Krozer V (2020). Numerical and experimental analysis of a transmission-based breast imaging system: a study of application to patients. *International Journal of Microwave and Wireless Technologies* **12**, 469–476. https://doi.org/10.1017/S1759078720000240

Received: 15 October 2019
Revised: 29 February 2020
Accepted: 3 March 2020
First published online: 7 April 2020

Key words:
Microwave imaging; image reconstruction; UWB diagnostics; patient study

Author for correspondence:
Somayyeh Chamaani,
E-mail: chamaani@eetd.kntu.ac.ir

Numerical and experimental analysis of a transmission-based breast imaging system: a study of application to patients

Elham Norouzzadeh[1], Somayyeh Chamaani[1], Jochen Moll[2], Christian Kexel[2], Duy Hai Nguyen[2], Frank Hübner[3], Babak Bazrafshan[3], Thomas J. Vogl[3] and Viktor Krozer[2]

[1]Department of Electrical Engineering, K. N. Toosi University of Technology, Tehran, Iran; [2]Department of Physics, Goethe University of Frankfurt, Frankfurt am Main 60438, Germany and [3]Institute for Diagnostic and Interventional Radiology, Goethe University Hospital Frankfurt am Main, Frankfurt am Main, Germany

Abstract

Early detection of breast cancer is required to increase the chances of a successful treatment. However, current breast-imaging systems such as X-Ray mammography, breast ultrasound, and magnetic resonance imaging have technological limitations so that novel solutions are needed to address this major societal problem. The current paper considers ultra-wideband (UWB) microwave radiation in the frequency band from 1 to 9 GHz. Given by the non-ionizing nature of microwaves frequent check-ups are more feasible. In this work, we propose algorithms for qualitative and quantitative microwave breast imaging for a transmission-based UWB system. Based on numerical and experimental data, the performance of the algorithms has been investigated and compared. Finally, microwave images obtained during an initial patient study are discussed relative to corresponding X-ray images.

Introduction

Latest developments in the area of microwave breast imaging consist of improving both the signal processing and image formation step [1–5] as well as the performance of data acquisition equipment [6–8]. Thanks to these advancements, different research groups have manufactured their pre-clinical imaging setups [9–13] aiming at breast screening in a larger number of women.

During the past two decades, the mortality rate caused by breast cancer has steadily decreased [14]. The reason for this trend can partly be explained by more women going through routine screening tests, such as X-ray mammography and magnetic resonance imaging (MRI). Given the ionizing radiation of X-rays, this type of mammography is confined to women over 40 years. On the other hand, due to the high costs of manufacturing and maintenance, screening by MRI devices is usually only recommended to women with a family history of breast cancer. These restrictions have forced researchers to look for other possibilities in order to compensate for the aforementioned limitations [15–18]. Microwave imaging systems have several advantages including cost-effectiveness, non-ionizing nature of microwave radiation, high dynamic range, availability of amplitude and phase information, and the ability to implement frequent check-ups [19–24]. In addition, microwave breast-imaging techniques may complement the diagnostic information about the tumors' microenvironment given by the analysis of the tumors' permittivity. A disadvantage is the larger wavelength of the microwave approach, so that recent developments aim at mm-wave breast-imaging systems which have a wavelength that is comparable with medical ultrasound systems [25].

While microwave tomography methods provide the permittivity map of breast tissue, they suffer from considerable computational expenses for solving the ill-conditioned inverse scattering problem [26]. Hence, it might be advantageous to consider radar-based microwave-imaging systems equipped with real-time image processing. However, many image reconstruction techniques have their own obstacles, e.g. assuming a constant and frequency independent relative permittivity [27, 24].

From the signal processing point of view, the aim of most radar-based methods is to synthetically focus the backscattered energy on the position of dominant scatterers [28]. In the case of breast imaging, the dominant scatterer could imply the presence of malignancy. Confocal methods such as delay and sum and delay multiply and sum [29, 30] are well recognized and have been used as standard techniques to assess performances of other image reconstruction schemes. A comparison of several digital beamforming techniques was proposed in [31]. Time-reversal-based algorithms also exhibit better performances in high cluttered medium and show promising results for breast tissues with severe inhomogeneities [32, 33]. Space-time beamforming methods claim that they are able to eliminate couplings between array elements and also compensate for path loss and frequency dispersion [34]. One of the main challenges in the implementation of all these methods is to make an efficient estimation of the relative permittivity of the breast tissue [35].

In this work, we introduce and compare qualitative and quantitative techniques for breast cancer imaging using a transmission-based imaging setup that operates in the frequency range from 1 to 9 GHz. The first algorithm follows the root-mean-square deviation (RMSD), analog to [24], to compute a qualitative breast-imaging map based on relative signal changes. The second algorithm uses, similar to [36], the differences between the time of arrival of electromagnetic waves propagating through air and breast tissue. However, the implementation of the phase center compensation is not needed here, because the transmitter and receiver are always aligned and move simultaneously to scan the breast tissue. This leads to a two-dimensional (2-D) map of estimated dielectric permittivity. In the third algorithm, the attenuation level of the transmission signals are computed and mapped to a 2-D image. This paper presents both, numerical results derived from simulation models and also clinical results obtained during an initial patient study. The experimental measurements are compared with X-ray mammograms of the same breast.

Experimental data acquisition

Figure 1 shows a schematic of our experimental setup which was previously introduced in [37]. The imaging system consists of two low loss plexiglass plates with 5 mm thickness used for breast compression. During the tests, the upper plate could move in the vertical direction to ensure a proper mechanical contact between the plates and the breast. Two ultra-wideband (UWB) bowtie antennas [38] for transmitting (top) and receiving (bottom) are connected to a HP 8720C vector network analyzer. Other UWB antenna sensors could have been used as well such as Vivaldi antennas [39], dipole antennas [40], wide-slot antennas [41], or dielectrically scaled horn antennas [42]. Measurements are performed in the frequency domain from 1 to 9 GHz using 101 frequency points with a sweep time of 90 ms. Next, the frequency domain measurements are transformed into time domain t using an inverse Fourier transform.

Both antennas can move in the horizontal direction to continuously scan a specified sensing volume in two dimensions. The measurement points and scan directions are depicted in Fig. 2 showing the meander-shaped scanning path. The whole system is controlled by an iPC25 (Isel, Eichenzell, Germany) using a Matlab interface. A measurement at coordinates (x, y) in the breast tissue is called $S(x, y; \omega)$ where ω represents the frequency. At the end of the scan a measurement in air is taken outside the breast region called $S_0(x, y; \omega)$.

The main advantages of our setup compared to related prototype systems are:

(i) no matching medium needed.
(ii) a mild breast compression is used to examine breasts with different size and geometry.
(iii) through a control unit it is possible to scan the breast tissue in a series of continuous points. Using only two antennas eliminates the need for a HF switching network.
(iv) simplified image reconstruction, because information on relative permittivity is not required.

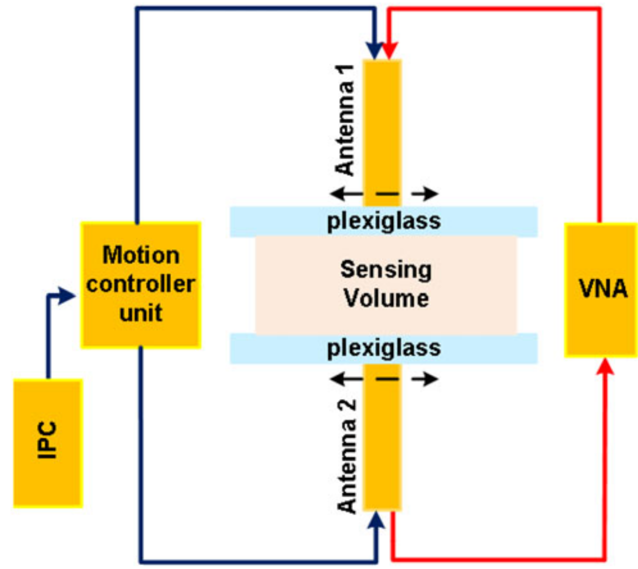

Fig. 1. Schematic of the experimental breast-imaging setup.

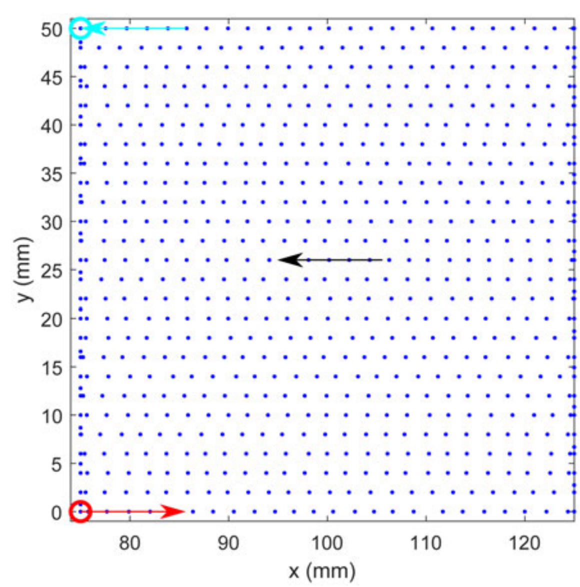

Fig. 2. Illustration of the spatial sampling during one breast scan. The scanning area is limited to 50 mm × 50 mm due to the limited examination time in the clinical study of 3 min.

Imaging algorithms

The numerical and experimental data are processed by three different imaging algorithms that are described below. Since the RMSD has been used for image formation in [37], not all results are presented in the results section.

Root-mean-square deviation

A qualitative 2-D microwave image $I_{RMSD}(x_i, y_j)$ can be computed by the RMSD according to

$$I_{RMSD}(x_i, y_j) = \sqrt{\frac{1}{\tau}\sum_{t=1}^{\tau}(s(x_i, y_j; t))^2} \tag{1}$$

https://doi.org/10.1017/S1759078720000240 Published online by Cambridge University Press

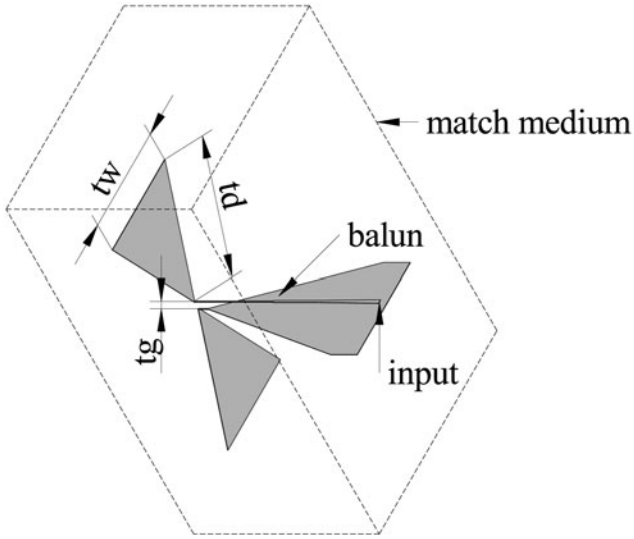

Fig. 3. Geometry of the bowtie antenna, after [44].

where the signal duration is expressed in samples and is denoted by τ. Here, x_i and y_i represent the Cartesian coordinates of the measurement position and $s(x_i, y_i; t)$ represents the time-domain radar signal recorded at (x_i, y_i).

Effective permittivity mapping

A quantitative 2-D microwave image can be obtained by a time difference analysis between a measurement in the breast $s(x_i, y_j; t)$ and a measurement in air $s_0(x, y; t)$. The time difference $\Delta t(x_i, y_j)$ between the first peaks maximum of $s(x_i, y_j; t)$ and $s_0(t)$ is computed and transformed into a permittivity map using the relationship:

$$\varepsilon_r(x, y) = \left(1 + \frac{\Delta t(x_i, y_j) \cdot c_0}{d}\right)^2 \tag{2}$$

where c_0 is the speed of light in free space and d is the separation distance between the antennas.

Attenuation mapping

The third method also leads to a quantitative 2-D microwave image. The algorithm computes the attenuation map $I(x_i, y_j)$ for

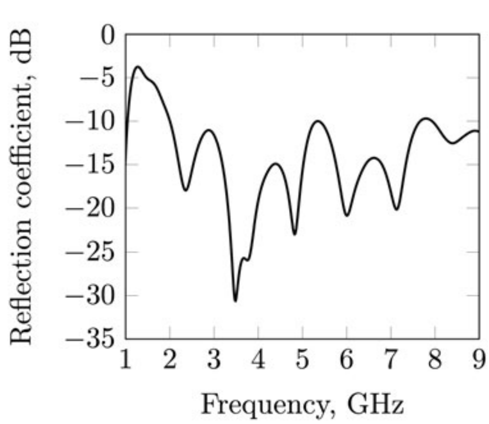

Fig. 4. Simulated reflection coefficient of a bowtie antenna, after [44].

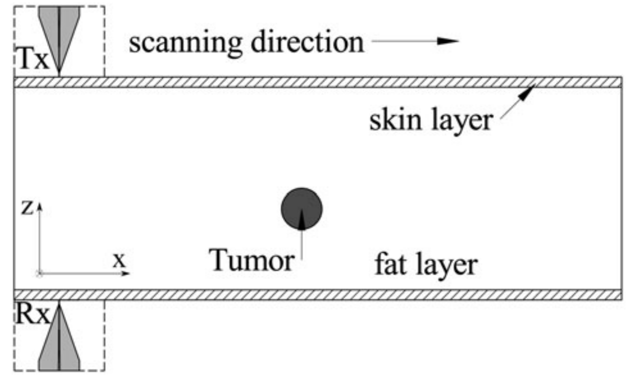

Fig. 5. Simulation setup for cancer tissue detection using two bowtie antennas (Tx–Rx).

every point in the imaging domain by processing the maximum of first peaks of corresponding transmission signals $\hat{s}(x_i, y_i; t)$ according to:

$$I(x_i, y_j) = -20\log\left(\frac{\hat{s}(x_i, y_j; t)}{\hat{s}(x, y; t)}\right) \tag{3}$$

The denominator serves as reference and is the global maximum of the first peaks of all signals.

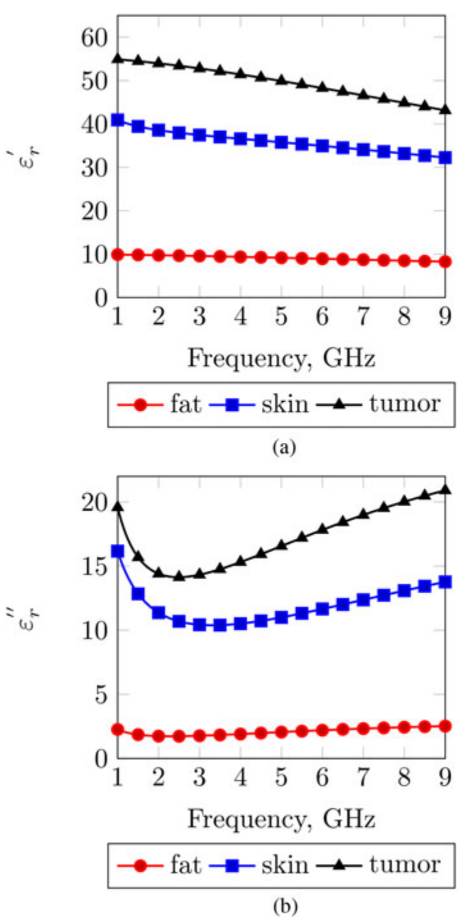

Fig. 6. Material properties of skin, fat, and tumor models, after [46].

https://doi.org/10.1017/S1759078720000240 Published online by Cambridge University Press

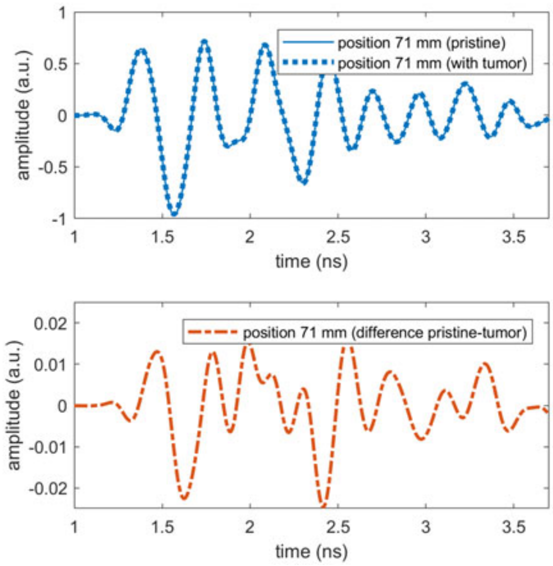

Fig. 7. Exemplary transmission signal at antenna position 71 mm from the numerical simulation (top row) with the corresponding deviation between the pristine and the scenario with tumor (bottom row).

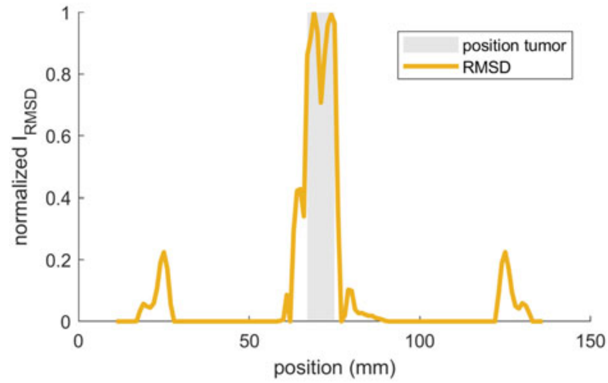

Fig. 8. RMSD of the numerical signals between the pristine and the scenario with tumor.

Numerical modeling

Description of the numerical model

In this section, we discuss a numerical model for malignant tissue detection in the frequency range from 1 to 9 GHz. The setup includes antennas as sensors, and a simplified numerical breast model for which the frequency-dependent material properties were derived from experimental measurements. Simulations are conducted by using CST Microwave Studio [43].

Antenna modeling

In this study, an UWB bowtie antenna [44] is used for the transmitter (Tx) and receiver (Rx) as shown in Fig. 3. The bowtie antenna has a width of $t_w = 9.9$ mm, length $t_d = 10.5$ mm, and a gap between two radiators of $t_g = 0.8$ mm. In order to transform the antenna's input impedance to 50 Ω, a tapered microstrip line (balun) is used. Furthermore, the bowtie antenna is designed to radiate into the patient's breast without a coupling medium. Assuming an average relative permittivity of $\varepsilon_r = 10$ the bowtie antenna is placed inside a matching solid medium, filled with Eccostock HiK ($\varepsilon_{rHiK} = 10$ [45]). Dimensions of the block are 22 mm × 35 mm × 17 mm ($w \times l \times h$).

Figure 4 shows the reflection coefficient at the antenna input. According to the figure, the antenna has a 10 dB return loss in the ultra-wideband frequency range from 2 to 9 GHz.

Detection scheme

A simplified numerical breast phantom for tumor detection is modeled and simulated. The main goal is to understand the behavior of the RMSD-based imaging technique in the proposed transmission-based imaging configuration. Figure 5 shows a 2-D view of the setup where the Tx and Rx face each other and move in one direction simultaneously along the x-direction. The antenna structure from the previous section is used for both sensors. Between the antennas is a homogeneous dispersive tissue, including skin and fat layers. Material properties are shown in Fig. 6 [46]. Each skin layer has a

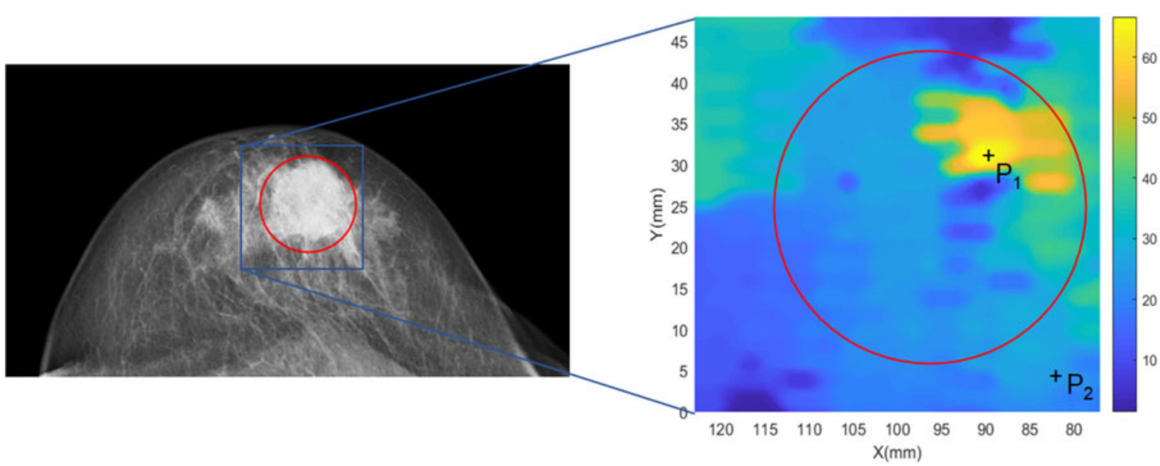

(a) (b)

Fig. 9. Comparison between X-ray image and microwave image for patient A. The microwave image is estimated through time delays caused by the propagation through the breast when compared to air. Locations with higher relative permittivity could be interpreted as cancerous tissue. The final thickness of the compressed breast is 44 mm during microwave examination and is 41 mm during X-ray examination.

https://doi.org/10.1017/S1759078720000240 Published online by Cambridge University Press

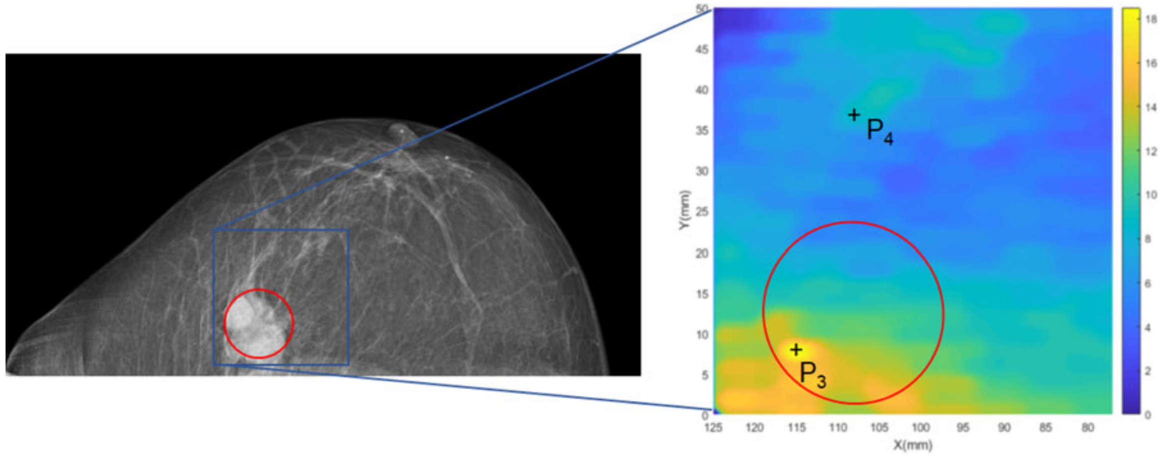

Fig. 10. Comparison between X-ray image and microwave image for patient B. The microwave image is formed by calculating the signal's attenuation. Locations with higher attenuation could be interpreted as cancerous tissue. The final thickness of the compressed breast is 43 mm during microwave examination and is 37 mm during X-ray examination.

thickness of $t_{skin} = 2.5$ mm, and the thickness of the fat layer is $t_{fat} = 50$ mm. In addition, both sensors contact directly to the skin surface. The scanning step is $d_{scan} = 1$ mm over 150 mm for maximum resolution.

The differential detecting procedure is divided into two steps:

(i) Baseline scanning (no tumors): the antennas scan along the sample, which does not have any cancer tissues. Transmission signals between Tx–Rx are set as references (baseline values).

(ii) Detection scanning (with tumor): in this scenario, a spherical tumor with diameter $\emptyset = 8$ mm is placed at position $x = 71$ mm. Transmission signals are recorded again and compared to the baseline signals.

Numerical results

In Fig. 7, an illustrative numerical time-domain signal is displayed. In order to explore the possibility to localize a tumor, the deviation between the tumor-free state and the state with tumor is considered. Therefore, the RMSD between both transmissions measurements is evaluated for all antenna positions according to equation (1). The early portion of the signal turns out to be particularly indicative. In Fig. 8, the normalized RMSD is plotted for all the antenna positions where below-average RMSD values have been zeroized. Therefore, at positions with a significant contribution to the RMSD the tumor can be localized.

Experimental results

In Figs 9(a) and 10(a) X-ray images of the breast tissues for patients A and B are displayed and the scanned regions of the breasts during microwave data acquisition are shown by blue rectangles. The scanning area is limited to 50 mm by 50 mm based on the ethics vote with the reference number 2/16 obtained from the ethics committee of the J.W. Goethe-Universitätsklinikum (Frankfurt am Main, Germany).

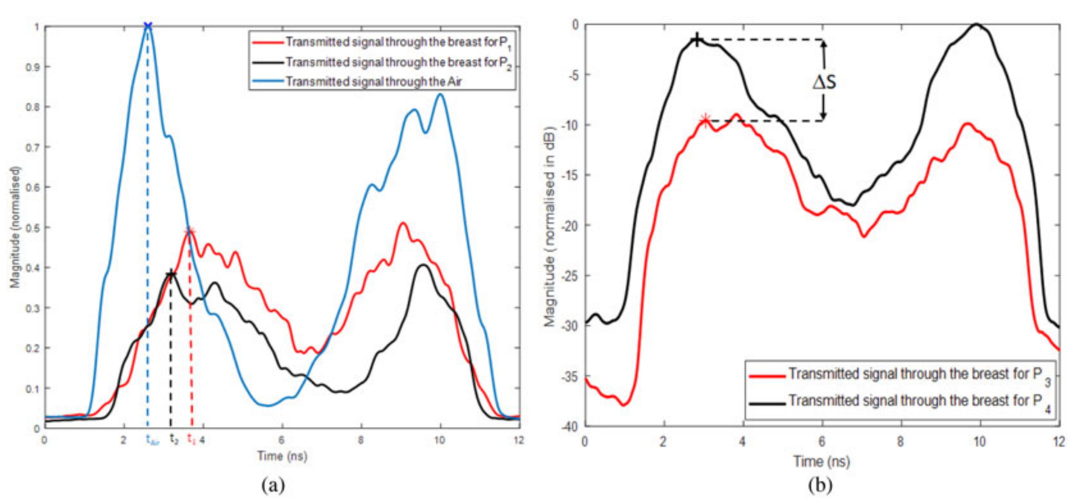

Fig. 11. (a) Exemplary transmission signals in patient A illustrating the variations in time of arrival; (b) transmission signals obtained from patient B illustrating variations in signal attenuation.

https://doi.org/10.1017/S1759078720000240 Published online by Cambridge University Press

Looking at Fig. 9(b), one can see the permittivity map using equation (2) for patient A. Compared with the corresponding X-ray image, the area with higher permittivity enclosed by the red circle can be determined as cancerous region. However, if we consider the parts confined by red circles in Figs 9(a) and 9 (b) we can see a variability of permittivity of malignant tissue which is in agreement with the obtained results of [28]. This result indicates that even cancerous regions have inhomogeneous dielectric properties.

The microwave attenuation image obtained using equation (3) for patient B is depicted in Fig. 10(b) and the zone with higher attenuation implies the tumor location. Comparing the microwave image confined in the red circle with its counterparts in the X-ray image confirms tumor existence. Like in the previous case, the attenuation of cancerous region is not constant.

An analysis on signal level is provided in Fig. 11(a) in which transmission signals in air are compared with transmission signals from two points in the breast of patient A, namely P_1 and P_2 as shown in Fig. 9(b). The time of arrivals for their first peaks are t_{Air}, t_1, and t_2. From these quantities the time difference Δt in equation (2) can be derived. In contrast to what we would have expected the time delay of the signal with the highest attenuation is not automatically the signal with greatest time delay. This fact can also be explained by the strong variability of dielectric properties of breast tissues obtained through spectroscopic studies [28; 47]. Another signal example is depicted in Fig. 11(b) showing transmission signals of patient B at the positions P_3 and P_4 shown in Fig. 10(b). The differences in peak amplitude of the first maximum is labeled as ΔS. The corresponding maxima are processed in equation (3) to compute the attenuation map.

Conclusions

This paper presented three image formation techniques for microwave breast imaging in a transmission-based configuration. A qualitative imaging was based on the RMSD. Two quantitative image reconstruction methods for UWB microwave breast imaging exploit variations in time delay for permittivity mapping and variations in amplitude for attenuation mapping, respectively. Besides a numerical breast phantom, initial results from a patient study have been presented and the results have been compared to X-ray mammography.

Acknowledgments. J.M., C.K., D.H.N., and V.K. gratefully acknowledge financial support of this research by the Federal Ministry of Education and Research (Grant Number: 13GW0361D).

References

1. **Foroozan F, HosseinKhah N and Adve R** (2018) Coherent time reversal sub-array processing for microwave breast imaging. *2018 IEEE International Conference on Acoustics, Speech and Signal Processing (ICASSP)*, Calgary TELUS Convention Centre, Calgary, Canada, pp. 3374–3378.
2. **Mukherjee S, Udpa L, Udpa S, Rothwell EJ and Deng Y** (2019) A time reversal-based microwave imaging system for detection of breast tumors. *IEEE Transactions on Microwave Theory and Techniques* **67**, 2062–2075.
3. **Abdollahi N, LoVetri J and Jeffrey I** (2019) A combined algorithm for high resolution microwave breast imaging using eigenfunction-based prior. *2019 13th European Conference on Antennas and Propagation (EuCAP)*, ICE Krakow Congress Centre, Krakow, Poland, pp. 1–3.
4. **Wang L** (2019) Multi-frequency holographic microwave imaging for breast lesion detection. *IEEE Access* **7**, 83984–83993.
5. **Tajik D, Trac J and Nikolova NK** (2019) Spatial resolution evaluation of a microwave system for breast cancer screening. *2019 13th European Conference on Antennas and Propagation (EuCAP)*, ICE Krakow Congress Centre, Krakow, Poland, pp. 1–5.
6. **Islam MT, Ullah MA, Alam T, Singh MJ and Cho M** (2018) Microwave imaging sensor using low profile modified stacked type planar inverted F antenna. *Sensors* **18**, 2949. [Online]. Available: https://www.mdpi.com/1424-8220/18/9/2949
7. **Wang L** (2018) Microwave sensors for breast cancer detection. *Sensors* **18**, 655. [Online]. Available: https://www.mdpi.com/1424-8220/18/2/655
8. **Wang L and Xu J** (2019) A new wideband microwave antenna for breast cancer detection. *American Society of Mechanical Engineers Digital Collection* [Online]. Available: https://asmedigitalcollection.asme.org/IMECE/proceedings/IMECE2018/52026/V003T04A040/273675
9. **Islam MT, Samsuzzaman M, Islam MT, Kibria S and Singh MJ** (2018) A homogeneous breast phantom measurement system with an improved modified microwave imaging antenna sensor. *Sensors* **18**, 2962. [Online]. Available: https://www.mdpi.com/1424-8220/18/9/2962
10. **Duchesne L, Fasoula A, Kaverine E, Robin G and Bernard J** (2019) Wavelia microwave breast imaging: identification and mitigation of possible sources of measurement uncertainty. *2019 13th European Conference on Antennas and Propagation (EuCAP)*, ICE Krakow Congress Centre, Krakow, Poland, pp. 1–5.
11. **Felicio JM, Bioucas-Dias JM, Costa JR and Fernandes CA** (2019) Microwave breast imaging using a dry setup. *IEEE Transactions on Computational Imaging* **6**, 167–168.
12. **Vispa A, Sani L, Paoli M, Bigotti A, Raspa G, Ghavami N, Caschera S, Ghavami M, Duranti M and Tiberi G** (2019) UWB device for breast microwave imaging: phantom and clinical validations. *Measurement* **146**, 582–589. [Online]. Available: http://www.sciencedirect.com/science/article/pii/S0263224119306116
13. **Wang F** (2019) *Wearable and Portable Radio Frequency Devices for Medical Microwave Imaging* (Ph.D. dissertation). The University of Edinburgh. [Online]. Available: https://www.era.lib.ed.ac.uk/handle/1842/35500
14. **Malvezzi M, Carioli G, Bertuccio P, Boffetta P, Levi F, La Vecchia C and Negri E** (2018) European cancer mortality predictions for the year 2018 with focus on colorectal cancer. *Annals of Oncology* **29**, 1016–1022.
15. **Garcia-Uribe A, Erpelding TN, Krumholz A, Ke H, Maslov K, Appleton C, Margenthaler JA and Wang LV** (2015) Dual-modality photoacoustic and ultrasound imaging system for noninvasive sentinel lymph node detection in patients with breast cancer. *Scientific Reports* **5**, 15748.
16. **Fakhrejahani E, Torii M, Kitai T, Kanao S, Asao Y, Hashizume Y, Mikami Y, Yamaga I, Kataoka M, Sugie T, Takada M, Haga H, Togashi K, Shiina T and Toi M** (2015) Clinical report on the first prototype of a photoacoustic tomography system with dual illumination for breast cancer imaging. *PLoS ONE* **10**, e0139113. [Online]. Available: https://journals.plos.org/plosone/article?id=10.1371/journal.pone.0139113
17. **Diot G, Metz S, Noske A, Liapis E, Schroeder B, Ovsepian SV, Meier R, Rummeny EJ and Ntziachristos V** (2017) Multi-spectral optoacoustic tomography (MSOT) of human breast cancer. *Clinical Cancer Research* clincanres.3200.2016. [Online]. Available: http://clincancerres.aacrjournals.org/content/early/2017/09/12/1078-0432.CCR-16-3200
18. **Ozmen N, Dapp R, Zapf M, Gemmeke H, Ruiter NV and van Dongen KWA** (2015) Comparing different ultrasound imaging methods for breast cancer detection. *IEEE Transactions on Ultrasonics, Ferroelectrics, and Frequency Control* **62**, 637–646.
19. **Chandra R, Zhou H, Balasingham I and Narayanan RM** (2015) On the opportunities and challenges in microwave medical sensing and imaging. *IEEE Transactions on Biomedical Engineering* **62**, 1667–1682.
20. **Meo SD, Espín-López PF, Martellosio A, Pasian M, Matrone G, Bozzi M, Magenes G, Mazzanti A, Perregrini L, Svelto F, Summers PE, Renne G, Preda L and Bellomi M** (2017) On the feasibility of breast cancer imaging systems at millimeter-waves frequencies. *IEEE Transactions on Microwave Theory and Techniques* **65**, 1795–1806.
21. **Modiri A, Goudreau S, Rahimi A and Kiasaleh K** (2017) Review of breast screening: toward clinical realization of microwave imaging. *Medical Physics* **44**, e446–e458.

22. **Oliveira BL, O'Loughlin D, O'Halloran M, Porter E, Glavin M and Jones E** (2018) Microwave breast imaging: experimental tumour phantoms for the evaluation of new breast cancer diagnosis systems. *Biomedical Physics & Engineering Express* **4**, 025036. [Online]. Available: http://stacks.iop.org/2057-1976/4/i=2/a=025036
23. **O'Loughlin D, O'Halloran MJ, Moloney BM, Glavin M, Jones E and Elahi MA** (2018) Microwave breast imaging: clinical advances and remaining challenges. *IEEE Transactions on Biomedical Engineering* **65**, 2580–2590.
24. **Wörtge D, Moll J, Krozer V, Bazrafshan B, Hübner F, Park C and Vogl TJ** (2018) Comparison of X-ray-mammography and planar UWB microwave imaging of the breast: first results from a patient study. *Diagnostics* [Online]. Available: https://www.ncbi.nlm.nih.gov/pmc/articles/PMC6164229/
25. **Prati M, Moll J, Kexel C, Nguyen D, Santra A, Aliverti A, Krozer V and Issakov V** (2020) Breast cancer imaging using a 24 GHz ultra-wideband MIMO FMCW radar: System considerations and first imaging results. *14th European Conference on Antennas and Propagation (EuCAP 2020)*, (accepted in December 2019).
26. **Kwon S and Lee S** (2016) Recent advances in microwave imaging for breast cancer detection. *International Journal of Biomedical Imaging* **2016**, 1–26. [Online]. Available: https://www.hindawi.com/journals/ijbi/2016/5054912/
27. **Moll J, Kelly T, Byrne D, Sarafianou M, Krozer V and Craddock I** (2014) Microwave radar imaging of heterogeneous breast tissue integrating a-priori information. *International Journal of Biomedical Imaging* **2014**, Article ID 94354910.
28. **Lazebnik M, Popovic D, McCartney L, Watkins CB, Lindstrom MJ, Harter J, Sewall S, Ogilvie T, Magliocco A, Breslin TM, Temple W, Mew D, Booske JH, Okoniewski M and Hagness SC** (2007) A large-scale study of the ultrawideband microwave dielectric properties of normal, benign and malignant breast tissues obtained from cancer surgeries. *Physics in Medicine and Biology* **52**, 6093–6115.
29. **Elahi MA** (2018) Confocal microwave imaging and artifact removal algorithms for the early detection of breast cancer. Thesis, NUI Galway, March. [Online]. Available: https://aran.library.nuigalway.ie/handle/10379/7290
30. **Sun YP, Zhang S, Cui Z and Qu LL** (2016) CS based confocal microwave imaging algorithm for breast cancer detection. *Technology and Health Care* **24**, S757–S765. [Online]. Available: https://content.iospress.com/articles/technology-and-health-care/thc1205
31. **Moll J, Kexel C and Krozer V** (2013) A comparison of beamforming methods for microwave breast cancer detection in homogeneous and heterogeneous tissue. *10th European Radar Conference (EuRAD)*, Utrecht, Netherlands, pp. 527–530.
32. **Hossain MD and Mohan AS** (2017) Cancer detection in highly dense breasts using coherently focused time-reversal microwave imaging. *IEEE Transactions on Computational Imaging* **3**, 928–939.
33. **Yousefnia M, Zadeh AE, Dehmollaian M and Madannejad A** (2018) A time-reversal imaging system for breast screening: theory and initial phantom results. *IEEE Transactions on Biomedical Engineering* **65**, 2542–2551.
34. **Bond EJ, Li X, Hagness SC and Veen BDV** (2003) Microwave imaging via space-time beamforming for early detection of breast cancer. *IEEE Transactions on Antennas and Propagation* **51**, 1690–1705.
35. **Martellosio A, Pasian M, Bozzi M, Perregrini L, Mazzanti A, Svelto F, Summers PE, Renne G, Preda L and Bellomi M** (2017) Dielectric properties characterization from 0.5 to 50 GHz of breast cancer tissues. *IEEE Transactions on Microwave Theory and Techniques* **65**, 998–1011.
36. **Bourqui J and Fear EC** (2016) System for bulk dielectric permittivity estimation of breast tissues at microwave frequencies. *IEEE Transactions on Microwave Theory and Techniques* **64**, 3001–3009.
37. **Wörtge D, Moll J, Mälzer M, Krozer V, Hübner F, Bazrafshan B, Vogl TJ, Santarelli A, Popović M and Nikolova N** (2018) Prototype system for microwave breast imaging: experimental results from tissue phantoms. *2018 11th German Microwave Conference (GeMiC)*, Freiburg, Germany, pp. 399–402.
38. **Moll J, McCombe J, Hislop G, Krozer V and Nikolova N** (2015) Towards integrated measurements of dielectric tissue properties at microwave frequencies. *2015 9th European Conference on Antennas and Propagation (EuCAP)*, Lisbon, Portugal, pp. 1–5.
39. **Çayören M, Abbak M and Akduman İ** (2014) Microwave breast phantom measurements with a cavity-backed Vivaldi antenna. *IET Microwaves, Antennas & Propagation* **8**, 1127–1133.
40. **Ley S, Helbig M and Sachs J** (2015) Preliminary investigations of magnetic modulated nanoparticles for microwave breast cancer detection. *Current Directions in Biomedical Engineering, Current Directions Biomed. Eng.,* **1**(1), 302–305.
41. **Gibbins D, Klemm M, Craddock I, Leendertz J, Preece A and Benjamin R** (2010) A comparison of a wide-slot and a stacked patch antenna for the purpose of breast cancer detection. *IEEE Transactions on Antennas and Propagation* **58**, 665–674.
42. **Schwarz U, Stephan R and Hein MA** (2010) Miniature double-ridged horn antennas composed of solid high-permittivity sintered ceramics for biomedical ultra-wideband radar applications. *2010 IEEE Antennas and Propagation Society International Symposium, July*. Toronto, ON: IEEE, pp. 1–4.
43. **Systemes D,** CST Studio Suite 2019. https://www.3ds.com/, 2002–2020.
44. **Moll J, McCombe J, Hislop G, Krozer V and Nikolova N** (2015) Towards integrated measurements of dielectric tissue properties at microwave frequencies. *2015 9th European Conference on Antennas and Propagation (EuCAP)*, Lisbon, Portugal, pp. 1–5.
45. ***Eccostock HiK 500F – High Temperature, Low Loss, Adjusted Dielectric Plastic*, Emerson & Cuming Microwave Products, 2014.**
46. **Martellosio A, Pasian M, Bozzi M, Perregrini L, Mazzanti A, Svelto F, Summers PE, Renne G, Preda L and Bellomi M** (2017) Dielectric properties characterization from 0.5 to 50 GHz of breast cancer tissues. *IEEE Transactions on Microwave Theory and Techniques* **65**, 998–1011.
47. **Goram S, Moll J, Wörtge D, Krozer V, Hübner F, Bazrafshan B and Vogl T**, (2018) Clinical investigation of breast biopsies: concurrent UWB microwave spectroscopy and ultrasound measurements. *12th European Conference on Antennas and Propagation*, London, UK, pp. 1–5.

Elham Norouzzadeh received her B.S. and M.S. degrees in electrical engineering in 2011 and 2014 from the Shahid Bahonar University of Kerman, Kerman, Iran and the Sharif University of Technology, Tehran, Iran, respectively. She is currently pursuing her Ph.D. degree in Electrical Engineering-Communication at the Department of ECE, K. N. Toosi University of Technology, Tehran, Iran. Her interests are UWB microwave imaging in biomedical applications, antenna and propagations, wireless and optical communications, and passive UWB Beamforming.

Somayyeh Chamaani received her B.S. degree in electrical engineering from the Sharif University of Technology in 2004 and her M.S. and Ph.D. degrees in electrical engineering from the K. N. Toosi University of Technology in 2006 and 2011. She joined K. N. Toosi University of Technology in 2011 as an Assistant Professor of Electrical Engineering. Her research focuses on UWB antennas; UWB identification; UWB sensing; and UWB localization.

Jochen Moll received his Dipl.Ing. and Ph.D. degrees in mechanical engineering from the University of Siegen, Germany, in 2007 and 2011, respectively. Presently, he is a Postdoctoral Research Assistant with Goethe University Frankfurt, Germany. His research interests include radar techniques for biomedical applications, signal processing, and imaging techniques. His research profile is located at http://www.jochenmoll.de.

Christian Kexel received his B.Sc. and M.Sc. in physics from Technical University Darmstadt, Germany and Goethe University Frankfurt, Germany, respectively. He is currently pursuing his Ph.D. degree in physics from Goethe University. His research interests include signal processing and imaging techniques.

Duy Hai Nguyen received his B.Eng. and M.Eng. in electrical engineering from the Frankfurt University of Applied Sciences, in 2012 and 2015, respectively. He is currently pursuing his Ph.D. degree in physics from Goethe University. His research focuses on antenna design for medical applications.

Frank Hübner received his Dipl.-Ing. degree in medical engineering from the Fachhochschule Gießen–Frberg, Giessen, Germany, in 2004, and his Ph.D. degree from Goethe-Universität Frankfurt, Frankfurt, Germany, in 2013. He was involved in medical imaging and diagnostic techniques including MRI and CT. Since 2005, he has been a Research Assistant with the Institute for Diagnostic and Interventional Radiology, Goethe-Universität Frankfurt. His current research interests include thermal ablation treatment procedures, especially laser-induced and microwave thermal therapies.

Babak Bazrafshan received his M.Sc. degree in physics from Universität Heidelberg, Heidelberg, Germany, in 2008, and his Ph.D. degree from the Department of Physics, Goethe-Universität Frankfurt, Frankfurt, Germany, in 2013. He was involved in medical imaging and diagnostic techniques including MRI and CT. Since 2013, he has been a Research Assistant with the Institute for Diagnostic and Interventional Radiology, Goethe-Universität Frankfurt. His current research interests include application of microwaves for thermal therapy and diagnostics, MRI-based methods for diagnostics, as well as the development of tissue-mimicking phantoms.

Thomas J. Vogl was born in Munich, Germany, in 1958. He received the Dr.Med. from the Ludwig Maximilian University of Munich (LMU), Munich, Germany, in 1983. In 1989, he was a Specialist in radiology with LMU, where he was a Senior Physician with the Radiological Clinic from 1990 to 1992. From 1992 to 1998, he was the Chief Senior Physician with Charité Berlin, Berlin, Germany, where he was a C3 Professor in 1993. Since 1998, he has been a Full Professor with Goethe-Universität Frankfurt, Frankfurt, Germany. His current research interests include interventional radiology cancer therapies such as transarterial chemoembolization and hyperthermia, as well as diagnostic radiology methods such as MRI- and CT-based diagnostic procedures. Dr. Vogl is member of several scientific associations and the Editorial Board of different scientific journals. He was a recipient of 13 national and international prizes and awards including the Hermann–Holthusen Ring from the Deutsche Röntgengesellschaft in 1994 and the Pater-Leander-Fischer Preis from the Deutsche Gesellschaft für Lasermedizin in 2003.

Viktor Krozer (M'91–SM'03) received his Dipl.-Ing. and Dr.-Ing. degrees in electrical engineering from Technical University Darmstadt, Darmstadt, Germany, in 1984 and 1991, respectively. In 1991, he was a Senior Scientist with Technical University Darmstadt working on high-temperature microwave devices and circuits and submillimeter-wave electronics. From 1996 to 2002, he was a Professor with the Technical University of Chemnitz, Germany. From 2002 to 2009, he was a Professor in electromagnetic systems, with DTU Elektro, Technical University of Denmark, and was the Head of the Microwave Technology Group. Since 2009, he has been an endowed Oerlikon-Leibniz-Goethe Professor in terahertz photonics with Goethe University Frankfurt, Frankfurt, Germany, and heads the Goethe-Leibniz-Terahertz-Center. He is also with Ferdinand-Braun-Institut (FBH), Berlin, Germany, leading the THz Components and Systems Group. His research interests include terahertz electronics, MMIC, nonlinear circuit analysis and design, device modeling, and remote sensing instrumentation.

https://doi.org/10.1017/S1759078720000240 Published online by Cambridge University Press